Quaternary Science Reviews 216 (2019) 34–46

Contents lists available at ScienceDirect

Quaternary Science Reviews

journal homepage: www.elsevier.com/locate/quascirev

High-resolution records of ^{10}Be in endogenic travertine from Baishuitai, China: A new proxy record of annual solar activity?

Hongyang Xu [a, b], Hiroko Miyahara [b, *], Kazuho Horiuchi [c], Hiroyuki Matsuzaki [d], Hailong Sun [e], Weijun Luo [e], Xiangmin Zheng [a], Yusuke Suganuma [f, g], Shijie Wang [e], Limin Zhou [a, h, **]

[a] School of Geographic Sciences, East China Normal University, Shanghai, 200062, China
[b] Humanities and Sciences/Museum Careers, Musashino Art University, Tokyo 187-8505, Japan
[c] Graduate School of Science and Technology, Hirosaki University, Hirosaki, Aomori 036-8561, Japan
[d] The University Museum, The University of Tokyo, 7-3-1 Hongo, Bunkyo-ku, Tokyo 113-0033, Japan
[e] State Key Laboratory of Environmental Geochemistry, Institute of Geochemistry, Chinese Academy of Sciences, Guiyang 550081, China
[f] National Institute of Polar Research, Midori-cho 10-3, Tachikawa, Tokyo 190-8518, Japan
[g] Department of Polar Science, School of Multidisciplinary Sciences, The Graduate University for Advanced Studies (SOKENDAI), Midori-cho 10-3, Tachikawa, Tokyo 190-8518, Japan
[h] Institute of Eco-Chongming, East China Normal University, Shanghai, 200062, China

ARTICLE INFO

Article history:
Received 31 January 2019
Received in revised form
10 May 2019
Accepted 14 May 2019
Available online 7 June 2019

Keywords:
Beryllium-10
Cosmogenic nuclide
Solar activity
Endogenic travertine

ABSTRACT

The accurate reconstruction of past solar activity is a prerequisite for assessing the role of solar forcing on climate variations. Cosmogenic ^{10}Be, produced by galactic cosmic rays and stored in natural archives such as ice cores and lake sediments, has been shown to be the most reliable as an indicator of past solar activity, although reconstructions at a higher, annual, resolution have remained elusive due to dating imprecision and uncertainties concerning the effect of depositional processes. Here, we employ a methodology that facilitates the annual reconstruction of past cosmic-ray and solar activity variations. An annual ^{10}Be record is assembled from an endogenic travertine in Baishuitai, China, covering the period 2001–2016 CE. We demonstrate that the effect of depositional processes when ^{10}Be is incorporated into travertine can be accounted for using the associated ^{9}Be and potassium (K) contents, and that the resulting corrected ^{10}Be content significantly correlates with the modeled global ^{10}Be production rates with a time lag of 1.5–2.5 years. Our results from the Baishuitai endogenic travertine suggest that the ^{10}Be record in such carbonate sediments has considerable potential as a high resolution proxy for past cosmic-ray and solar activity variations.

1. Introduction

Solar activity is an important natural driving force of climate variations and a more complete understanding of solar activity in the past enables more reliable quantitative evaluations of solar influence on climate. It is well known that the sun has multi-decadal to multi-millennial variations in addition to the basic eleven-year solar cycle (see, for example, reviews by Beer et al., 2006; Usoskin, 2017). However, even the longest continuous observational records of sunspots only extend to around 400 years ago, and are too short to assess the precise history of solar activity during the Holocene epoch. With the development of Accelerator Mass Spectrometry (AMS), several studies of the cosmogenic radionuclide Beryllium-10 (^{10}Be) have yielded important longer-term information on the past solar activity (Beer et al., 1990; Vonmoos et al., 2006; Steinhilber et al., 2012; Muscheler et al., 2016; Wu et al., 2018).

Cosmogenic ^{10}Be is produced mainly in the lower stratosphere and the upper troposphere by the cosmic-ray induced spallation reaction involving atmospheric components such as N and O atoms (Lal and Peters, 1967). The atmospheric production rate of ^{10}Be is

* Corresponding author. Humanities and Sciences/Museum Careers, Musashino Art University, Tokyo 187-8505, Japan.
** Corresponding author. School of Geographic Sciences, East China Normal University, Shanghai, 200062, China.
E-mail addresses: miyahara@musabi.ac.jp (H. Miyahara), lmzhou@geo.ecnu.edu.cn (L. Zhou).

https://doi.org/10.1016/j.quascirev.2019.05.012
0277-3791/

proportional to cosmic ray intensity, which is modulated largely by variations in solar activity and the strength of the geomagnetic field (Lal and Peters, 1967). Following its production, ^{10}Be is attached to aerosols and is transported to the troposphere, where it is removed from the air primarily by precipitation (Beer et al., 2013). The stratospheric residence time of ^{10}Be is 1–2 years and it allows homogeneous mixing, while the tropospheric residence time of ^{10}Be is within a few months and it results in the regional difference in ^{10}Be precipitation amount (Raisbeck et al., 1981a; Heikkila et al., 2011).

A number of different ^{10}Be series have been published that have been applied to the study of past solar activity, for example from polar ice cores (Raisbeck et al., 1981b; Beer et al., 1988; Bard et al., 1997; Vonmoos et al., 2006; Berggren et al., 2009; Delaygue and Bard, 2010; Cauquoin et al., 2014; Horiuchi et al., 2008, 2016), mountain ice cores (Inceoglu et al., 2016), and lake sediments (Ljung et al., 2007; Berggren et al., 2010, 2013; Mann et al., 2012; Czymzik et al., 2015, 2016, 2018). Other studies have examined the influence of changes in solar activity on climate (Gray et al., 2010; Yamaguchi et al., 2010; Steinhilber et al., 2012).

However, there are several challenges to the interpretation of the ^{10}Be record in ice cores and lake sediments, especially to in achieving more precise – annual-resolution. For example, it has been reported that the ^{10}Be records from different ice cores exhibit a certain degree of differences in their variations, attributed to short-term climate impacts on ^{10}Be transportation and deposition processes (Berggren et al., 2009; Baroni et al., 2011; Pedro et al., 2012). Obtaining a high-resolution data using ice core is also a challenge, especially at greater depth where the annual layer thickness decreases by the thinning effect (Beer, 2000). Some authors have attempted higher resolution solar activity reconstructions using lake sediments (Berggren et al., 2010, 2013; Czymzik et al., 2015, 2018). In the case of lake sediments, depositional processes are even more complex than in ice cores (Horiuchi et al., 2001, 2003), and the methodology to extract atmospheric ^{10}Be content need to be further explored (Berggren et al., 2013; Czymzik et al., 2018). In addition, due to the generally slow rate of lake sediment deposition, only a few studies have attempted to interpret the ^{10}Be signal at an annual resolution. Accordingly, improved, or new, methodologies are needed to deliver high resolution past cosmic-ray and solar activity variations at the annual scale.

Travertines are widespread terrestrial carbonates formed in rivers/streams, and are among the most important continental climate-related deposits (Pentecost, 1995; Ford and Pedley, 1996; Andrews, 2006; Liu, 2014). They exhibit high deposition rates of several millimeters to more than a centimeter per year, and these characteristics suggest they are potential archives to trace past solar activity at high temporal resolution. In the case of travertines, thinning effect is negligibly small. Until now, however, the ^{10}Be record preserved in annually laminated travertine has not been applied to the reconstruction of solar activity.

In this paper, we describe a 16-year-long annual ^{10}Be record from endogenic travertine in Baishuitai, China, covering the period 2001–2016 CE (hereafter 2001–2016). The resulting ^{10}Be time-series is corrected for environmental proxy records from the same archive to constrain the process of ^{10}Be deposition in the travertine sediment, and compared with the modeled global ^{10}Be production rate to evaluate its potential for quantitative reconstruction of solar activity.

2. Materials and methods

2.1. Sampling site

Baishuitai is located in Shangri-La County, northwestern Yunnan Province, southwest China (Fig. 1), some 50 km distant from Shangri-La City and is at an elevation of around 2380–3800 m (Zhao et al., 1998). The area is characterized by a subtropical monsoon climate, with >75% of the annual precipitation (approximately 750 mm) occurring during the rainy season from May to October and has an annual mean air temperature of around 8 °C. Besides, Baishui River, a tributary of Jinsha River, traverses this area (Liu et al., 2003; Sun et al., 2014). The geomorphology of the Baishuitai area is characterized by a typical constructive karst landscape formed from limestone of the Triassic Beiya Formation. Due to intensive geotectonic activity and rock weathering, this limestone is highly fractured, and many faults and fissures have been developed which have provided good conditions for rainfall infiltration and groundwater inflow. Owing to the existence of a fault-controlled drainage cut-off, there are numerous springs upwelling at an altitude of about 2600 masl, including those labelled S1, S2 and S3 in Fig. 1 (Liu et al., 2003).

Previous studies have confirmed the formational processes of travertine in Baishuitai (Liu et al., 2003, 2006, 2016). As a consequence of the regional limestone geology, precipitation percolates the subterranean system and ultimately emerges as spring water upwelling at the surface, enriched in concentrations of HCO_3^- and Ca^{2+} ions. Subaerially, this spring water then forms the travertine following CO_2 degassing. Because there are strong seasonal variations in the amount of precipitation, the travertine has developed clear visible layers. During the rainy season, heavy local precipitation dilutes the spring water, and reduces the travertine deposition rate while at the same time inducing the incorporation of additional materials derived from eroded soils and sediments transported in the overland flow. These processes result in the accumulating travertine layers being thinner and darker brown in color. During the dry season, the deposition rate of travertine increases due to the higher rate of evaporation and this, coupled with lower quantities of mineral sediment, makes the travertine layer both thicker and paler in color. Since the main water source is spring water supplied from precipitation, this continuously adds atmospheric ^{10}Be to the travertine. Environmental conditions at Baishuitai combine to produce particularly clear visible annual layers and, therefore, make this travertine especially suited to the analysis and interpretation of incorporated ^{10}Be at an annual resolution.

In this study, we used the travertine deposited in an artificial canal in Baishuitai, which was constructed in May 1998 (Liu et al., 2016) (Fig. 1). In the dry season (November to April), the primary water source of the canal is the S3 spring, while this source is diluted by the water flow from the Baishui River, as well as direct local precipitation, during the rainy season (May to October). Despite these seasonal variations in the main water sources, the actual discharge is perennial and varies only slightly (~50–60 L/s) from month to month depending on the timing, duration and intensity of the monsoon (Sun and Liu, 2010).

2.2. Sampling

The travertine profile was obtained from the artificial canal at Baishuitai (27°30′14.2″N, 100°2′14.7″E), approximately 500 m distant from the S3 spring, in July 2017 (Fig. 1). The sample profile is approximately 30 cm in length (Fig. 2a) and is characterized by a soil layer at the top and a mixture of soil and gravel at the base. A clear laminated structure is evident, with a sequence of thicker white or paler colored layers sandwiched between thinner brown layers (Fig. 2a).

After drying the material at 60 °C for three days, the sample was divided into several smaller blocks, one of which (Fig. 2b) was used in this study. After cleaning the surface of the block, we identified

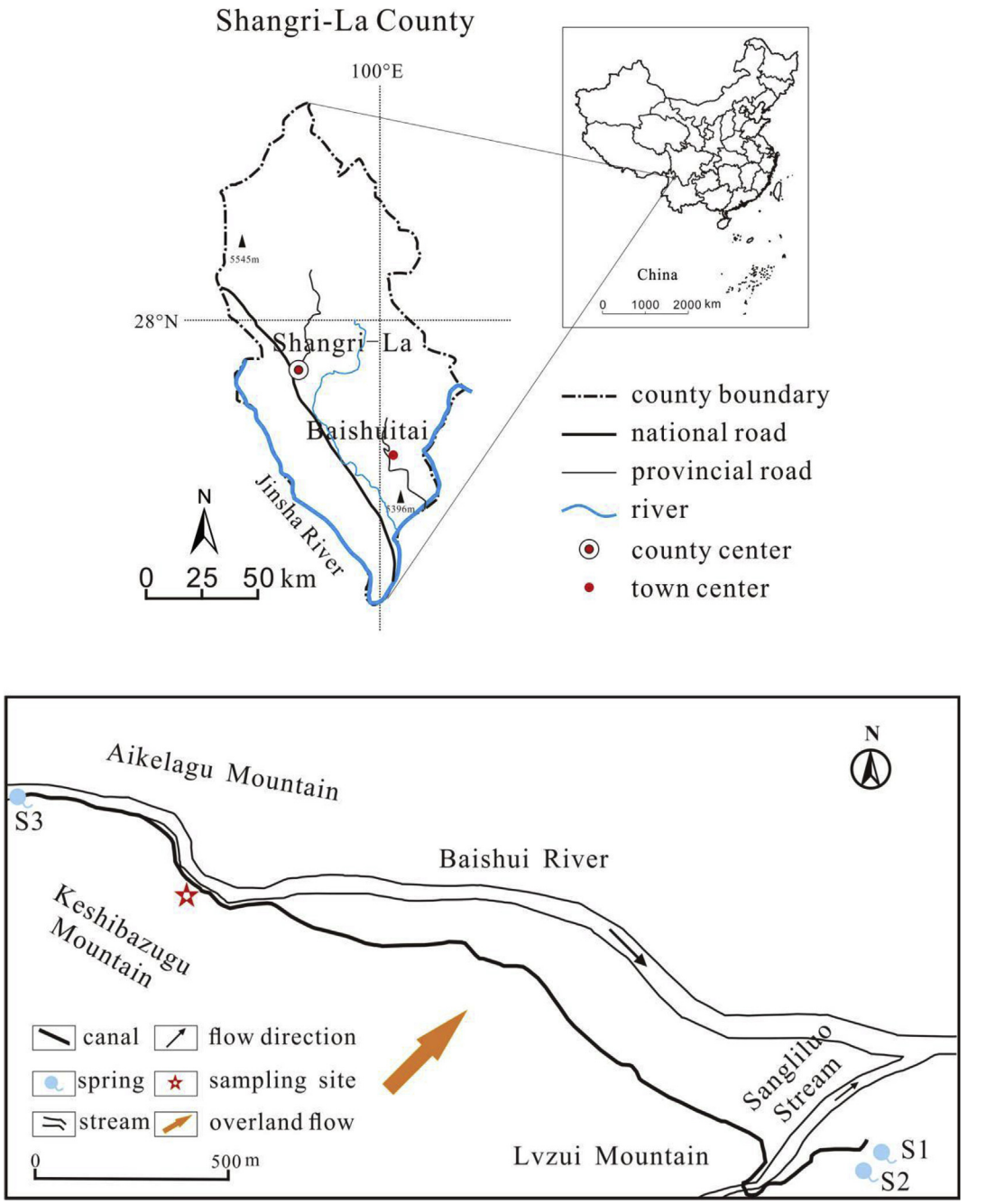

Fig. 1. The geographical location of Baishuitai, Yunnan Province, southwest China and the travertine sampling site (after Sun and Liu. (2010) and Liu et al. (2016)).

16 clear white layers and 16 dark layers across its 30 cm length. Following the cutting method as shown in Fig. 2c (For the detailed information, see Supplement 1), we cut the block with a slab saw, and obtained 16 individual white (W1 to W16), 16 dark (D0 to D15) layer samples.

In this study, we focus on the W-series samples that are less contaminated with material from overland flow as noted in section 2.1 above. Each of the individual samples was ground to powder in a stainless-steel mortar for subsequent analysis.

2.3. Dating

The travertine in Baishuitai reveals obvious characteristics of seasonal variation. As noted above, white thick layers are formed during the dry season, while the thin dark layers, incorporating soils and sediments, are deposited during the rainy season. Thus, one white/dark layer pair accounts for a single year of deposition, thereby allowing us to date the travertines simply by counting the number of the paired layers (Liu et al., 2016).

We first determined the age of the top white layer in the travertine profile (Fig. 2b). The artificial canal in Baishuitai was rebuilt in the summer of 2016, constructing a sealed tube in the canal, into which all discharge is now channelled, thus preventing further deposition of travertine in the canal. Therefore, the top white layer can be considered as having been formed around November 2015 to April 2016. Given that the main formational period of the top white layer travertine is in 2016, we designated the top white layer as 2016 in this study.

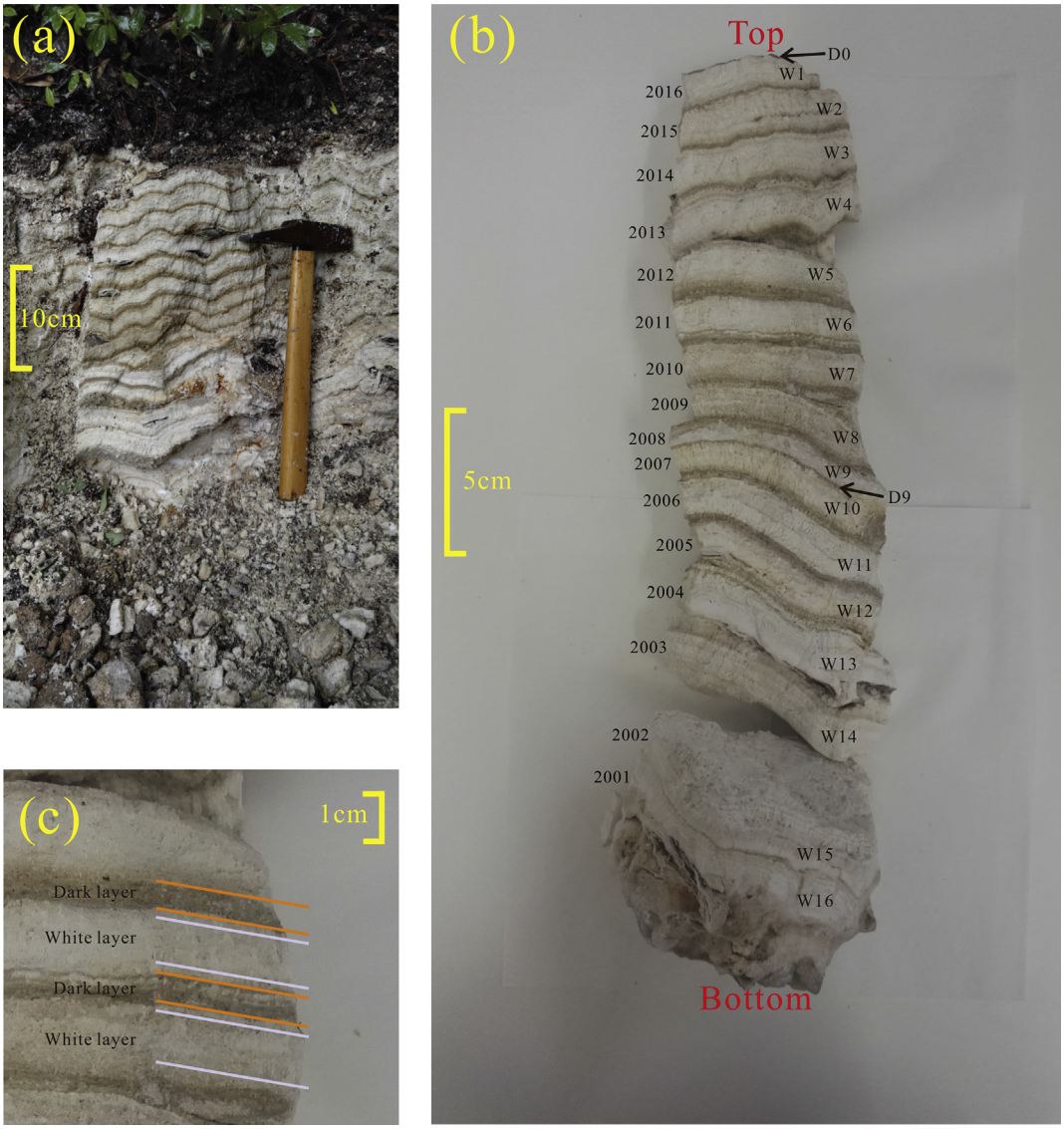

Fig. 2. (a) The laminated structure of the travertine profile; (b) A subdivided block used in this research; (c) Close-up of sub-sampling method. In panel c, the areas between the two nearby orange lines represent the layers of travertine formed at rainy season while the areas between the two white lines represent the layers of travertine formed during dry season. The areas between adjacent orange and white lines represent the removed parts. The approximate lengths of removed parts were less than 10% of the correspondent white layer (For the detailed information, see Supplement 1). (For interpretation of the references to color in this figure legend, the reader is referred to the Web version of this article.)

Since the opening of canal in 1998, the travertine in the canal has accumulated continuously without significant interruption (Liu et al., 2016). We therefore dated the rest of the layers by counting the pairs of white and dark layers, without complications, except that the dark layer (D9) between W9 and W10 is much thinner than other equivalents (Fig. 2b). Given this situation, two age models are possible: a) both layers accumulated in 2008 (age model 1: AM1), and b) the layers accumulated in different years, 2007 and 2008, as shown in Fig. 2b (age model 2: AM2). In order to confirm which of the age models to accept, we used the Pearson's correlation coefficient (R) (For the detailed illustration of this method, see Section 3.1.2) to assess the thickness and oxygen isotope ratios in relation to recorded precipitation and temperature values obtained from the meteorological station of Shangri-La, about 50 km from the sample site (Fig. 1).

First, we compared the thickness of white layers with dry season precipitation, since carbonate thickness, and hence accumulation rate, is negatively correlated with precipitation (Liu et al., 2006; Sun and Liu, 2010). In the case of AM2 (Fig. 3b), there is a significant negative correlation ($R = -0.66$ with 87% (1.5σ) confidence interval (CI) of -0.91 to -0.15), while AM1 yields less significant positive correlation ($R = 0.40$ with 87% CI of -0.20 to 0.69) (Fig. 3a). In addition, we compared the thickness of white layer with dry season temperatures. Carbonate accumulation rate increases with dry season temperature (Liu et al., 2010, 2016). The comparison reveals a significant positive correlation in the case of AM2 ($R = 0.54$ with 87% CI of 0.02–0.81) (Fig. 3d), and a clear negative correlation in AM1 ($R = -0.54$ with 87% CI of -0.84 to -0.01) (Fig. 3c). The analysis therefore confirms that AM2 is the more appropriate and that the W9 and the W10 were formed in 2008 and 2007, respectively.

Further confirmation was obtained by comparing the $\delta^{18}O$ value of the intervening dark layer with rainy season precipitation. Due to the amount effect, $\delta^{18}O$ is decreased as precipitation increases (Dansgaard, 1964). In AM2, rainy season $\delta^{18}O$ is indeed negatively correlated ($R = -0.44$ with 87% CI of -0.77 to -0.02) (Fig. 3f), while

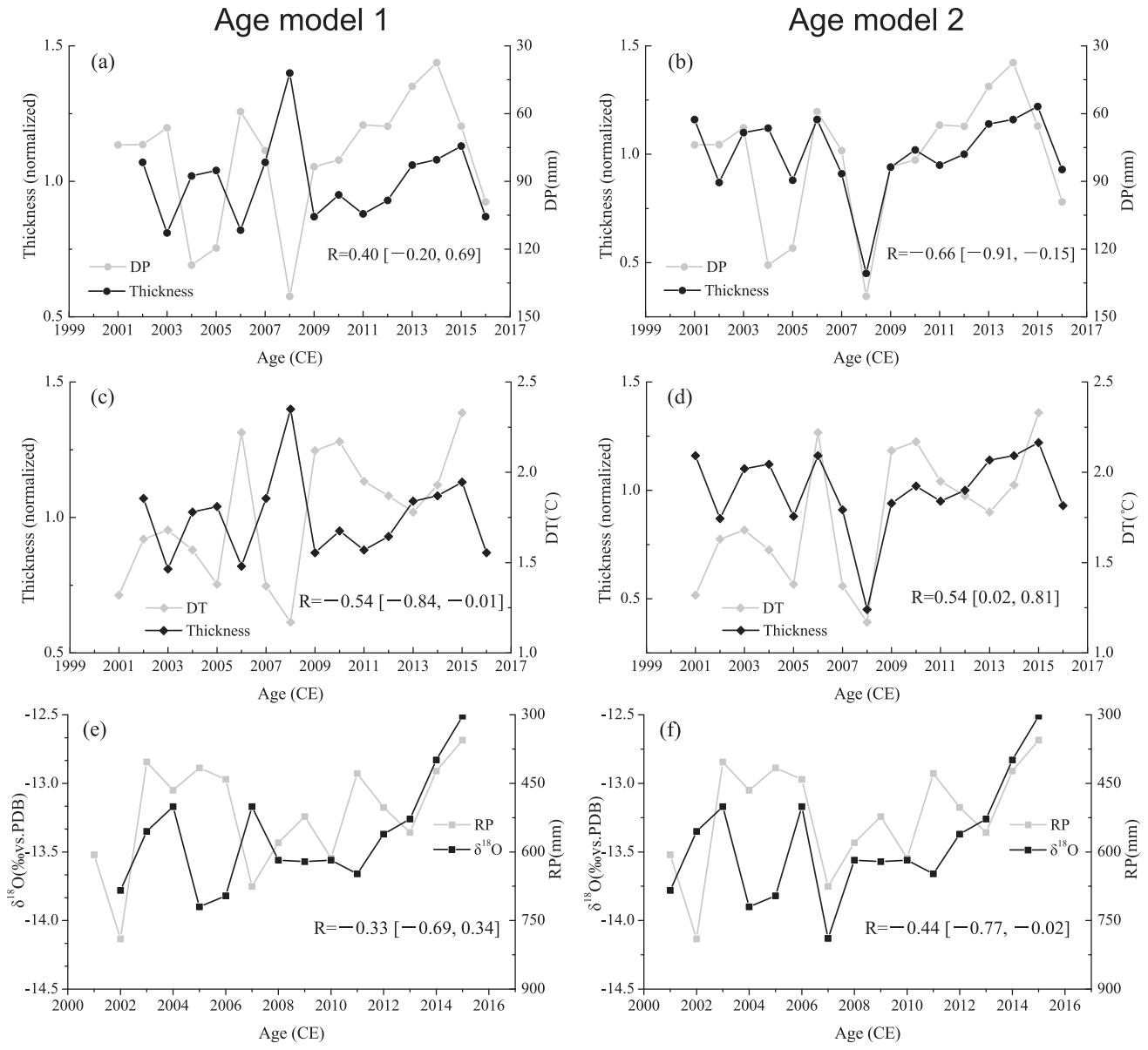

Fig. 3. Comparison of travertine profiles with environment proxy records based on two suggested possible age models. (a) Comparison between the thickness of white layers and dry season precipitation (DP) for age model 1 (AM1); (b) As in (a) but for age model 2 (AM2); (c) Comparison between the thickness of white layers and dry season temperature (DT) for AM1; (d) As in (c) but for AM2; (e) Comparison between $\delta^{18}O$ of dark layer and rain season precipitation (RP) for AM1; (f) As in (e) but for AM2. Correlation coefficient (R) is indicated together with the 87% (1.5σ) confidence intervals (CI). Note that right-hand axes in (a), (b), (e) and (f) are inverted. Precipitation and temperature data are derived from China Meteorological Administration, URL: https://data.cma.cn/.

for AM1 the negative correlation is comparatively weaker (R = −0.33 with 87% CI −0.69 to 0.34) (Fig. 3e), when the dating is 1-year different from AM2. This comparison therefore also supports the application of AM2 as the most likely scenario and hereafter we treat W9 and W10 as independent samples that accumulated in 2008 and 2007, respectively. Accordingly, the travertine covers the period 2001–2016, and totals 16 years (Fig. 2b).

2.4. *^{10}Be extraction and AMS measurements*

Sub-samples of 3 g from each powdered layer were accurately weighed and dissolved in 150 ml of 10% acetic acid (CH_3COOH). After agitating at 50–60 °C for 30 min in an ultrasonic wave cleaner, the dissolved sample was centrifuged for 15 min at 3000 rpm. Only the clear supernatant was subsequently used, from which an aliquot was taken to analyze the trace element content.

The sample solutions were then spiked with 150 μg of an accurately weighed ^{9}Be carrier (1500 μL of a 100-ppm Be standard solution supplied by Wako Pure Chemical Industries., Ltd., Osaka, Japan), evaporated to dry on a hot plate, and fumed with a nitric acid/perchloric acid ($HNO_3/HClO_4$) mixture. The residue was subjected to anion and cation exchange to extract the Be^{2+} fraction. $Be(OH)_2$ was precipitated from the eluted fraction by adding ammonia water ($NH_3 \cdot H_2O$) and washed twice with deionized water (~15 MΩcm resistivity). It was then dried in a quartz cup on a hot plate, followed by conversion to BeO via heating in a microwave crucible (Horiuchi et al., 2013; Horiuchi and Matsuzaki, 2015). BeO was mixed with Nb powder and pressed into a copper cathode for subsequent ^{10}Be AMS analysis. All the chemical treatments described above were conducted at the Paleoenvironmental and

Cosmogenic Nuclide Laboratory at Hirosaki University.

^{10}Be content was measured at the Micro Analysis Laboratory, Tandem Accelerator, University of Tokyo (MALT) (Matsuzaki et al., 2004, 2015). We used the KN standard (Nishiizumi et al., 2007) with a nominal ^{10}Be/^{9}Be ratio of 8.56×10^{-12} to normalize the data. The process blanks had a^{10}Be/^{9}Be ratio of 1×10^{-14}, whereas the samples had ^{10}Be/^{9}Be ratios ranging between 3.5×10^{-14} and 12×10^{-14}. The precision of the data was estimated from the propagation of the standard deviations of the sample and process blank counting statistics and the sample standard deviation for replicated measurements of the ^{10}Be standards.

2.5. Elemental composition and isotope measurements

Using the initial centrifuge supernatant from each sample, ^{9}Be content was determined using graphite furnace atomic absorption spectrometry on a Hitachi Z-2710 or Hitachi ZA3700 (Hitachi High-Tech Science Corporation, Tokyo, Japan) in the Paleoenvironmental and Cosmogenic Nuclide Laboratory at Hirosaki University according to the procedures described by Horiuchi et al. (2016). Content of potassium (K) and other metallic elements in the same supernatant were determined using ICP-OES (Varian 710-ES) in School of Geographic Sciences, East China Normal University. Isotopes (δ^{18}O, δ^{13}C) were measured using a Finnigan MAT252 instrument at the Institute of Geochemistry, Chinese Academy of Sciences according to the procedures described in Sun and Liu (2010). Standard deviation (1σ) values of the isotopic measurements were 0.15‰ for δ^{13}C and 0.20‰ for δ^{18}O.

3. Results and discussions

3.1. Characteristics of ^{10}Be in travertine

3.1.1. ^{10}Be concentration and flux

Concentrations of ^{10}Be (hereafter ^{10}Be$_{con}$) in all of the 16 white layers from 2001 to 2016 are shown in Table 1. The annual ^{10}Be$_{con}$ ($\pm 1\sigma$) varies between $1.23 \pm 0.13 \times 10^5$ atoms g^{-1} and $3.79 \pm 0.19 \times 10^5$ atoms g^{-1}, with a mean of $2.11 \pm 0.15 \times 10^5$ atoms g^{-1}.

Based on the ^{10}Be flux calculation method (For the detailed information, see Supplement 2), we estimated the approximate ^{10}Be$_{flux}$ for the travertine range from 186 to 447 atoms m^{-2} s^{-1} (Table 1). These results are broadly consistent with the estimated precipitation rates of ^{10}Be in the vicinity of the sampling site according to Heikkila et al. (2011), who suggest flux values of approximately 180–360 atoms m^{-2} s^{-1} between latitudes 20°N and 40°N.

Table 1
Results of measurements of the ^{10}Be concentration and calculated ^{10}Be flux. Note that the actual depositional period is from November of the previous year to around April of the year.

Year (CE)	^{10}Be concentration (10^5 atoms g^{-1})	Error (1SD)	^{10}Be flux (atoms m^{-2} s^{-1})
2016	2.05	0.14	250
2015	1.31	0.15	208
2014	1.23	0.13	186
2013	2.09	0.13	310
2012	1.98	0.14	259
2011	1.91	0.14	236
2010	3.07	0.19	407
2009	3.65	0.20	447
2008	3.79	0.19	222
2007	2.03	0.12	241
2006	1.31	0.11	198
2005	1.70	0.11	195
2004	1.81	0.14	263
2003	1.78	0.14	255
2002	1.88	0.15	214
2001	2.13	0.15	321

The ^{10}Be flux from most of the terrestrial sediments, including lake sediments, are usually not 1:1 related to the atmosphere deposition flux. For example, the ^{10}Be flux obtained from Lake Tiefer See and the Lake Czechowskie are one order of magnitude higher than the atmospheric deposition flux (Czymzik et al., 2015). It is because the transportation process of ^{10}Be involves the attachment of precipitated ^{10}Be to the clastic silicate materials, and the aggregation of such materials around the catchment area. In this study, we find that the ^{10}Be flux retrieved from the travertines are more or less directly reflecting the atmospheric deposition flux. We speculate that this may be because the affinity of calcium carbonate (or the ions of HCO_3^-) to beryllium is extremely low and that ^{10}Be keeps flowing around the watershed in the forms of $BeOH^+$, $Be(OH)_2$ or Be^{2+}. In such case, the temporal variations of ^{10}Be flux to be retrieved from the sediment is insusceptible to those of sediment composition or focusing by clastic materials.

3.1.2. The relationship between ^{10}Be$_{con}$ and the global ^{10}Be production rate

To assess the potential of travertine ^{10}Be as a proxy to reconstruct the past solar activity, we compared the time series with the global ^{10}Be production rate. For the comparison, we calculated the annual global ^{10}Be production rate based on the relationship between the global ^{10}Be production rate and the solar modulation parameter for cosmic rays provided by Poluianov et al. (2016). Here, we applied their model, in which geomagnetic dipole moment $M = 7.8 \times 10^{23}$ A m^2 is assumed. For the solar modulation parameter, we used the values provided by Usoskin et al. (2011) that are available at https://cosmicrays.oulu.fi/phi/phi.html.

In order to quantify the degree of correlation between the ^{10}Be time series and the modeled production rate, we conducted the Pearson's correlation analysis in this study. We employ a non-parametric stationary bootstrap method to calculate the correlation coefficient (R) and the associated 95% (bias-corrected and accelerated) confidence intervals (CI). Note that if the CI crosses zero then the correlation is not significant at 95%. This approach provides reliable results when applied to autocorrelated data (Mudelsee, 2003). This method has also been successfully applied to the ice core ^{10}Be records (Pedro et al., 2011, 2012).

Given that the approximate atmospheric residence time of ^{10}Be is about 1–2 years (Raisbeck et al., 1981a), and there could also be additional delay in the process of deposition into travertine, it is expected that ^{10}Be lags the global ^{10}Be production rate by one to a few years.

Fig. 4a shows the results for the Baishuitai travertine indicating a significant maximum correlation between the two variables ($R = 0.63$ with 95% CI of 0.09–0.83) with a lag of 0.5 year (See Fig. S2(a)), suggesting that ^{10}Be concentrations do indeed reflect the atmospheric radionuclide production signal. Note that ^{10}Be concentration is shifted by a half year into the past in Fig. 4a according to the lag analysis.

However, ^{10}Be concentrations in travertine are likely to be influenced by factors relating to depositional processes. We therefore further explored such possible effects, as outlined below.

3.2. The effect of accumulation rate and its correction

Initial observations suggest that rainy season ^{10}Be concentrations are generally higher than in the dry season, resulting mainly

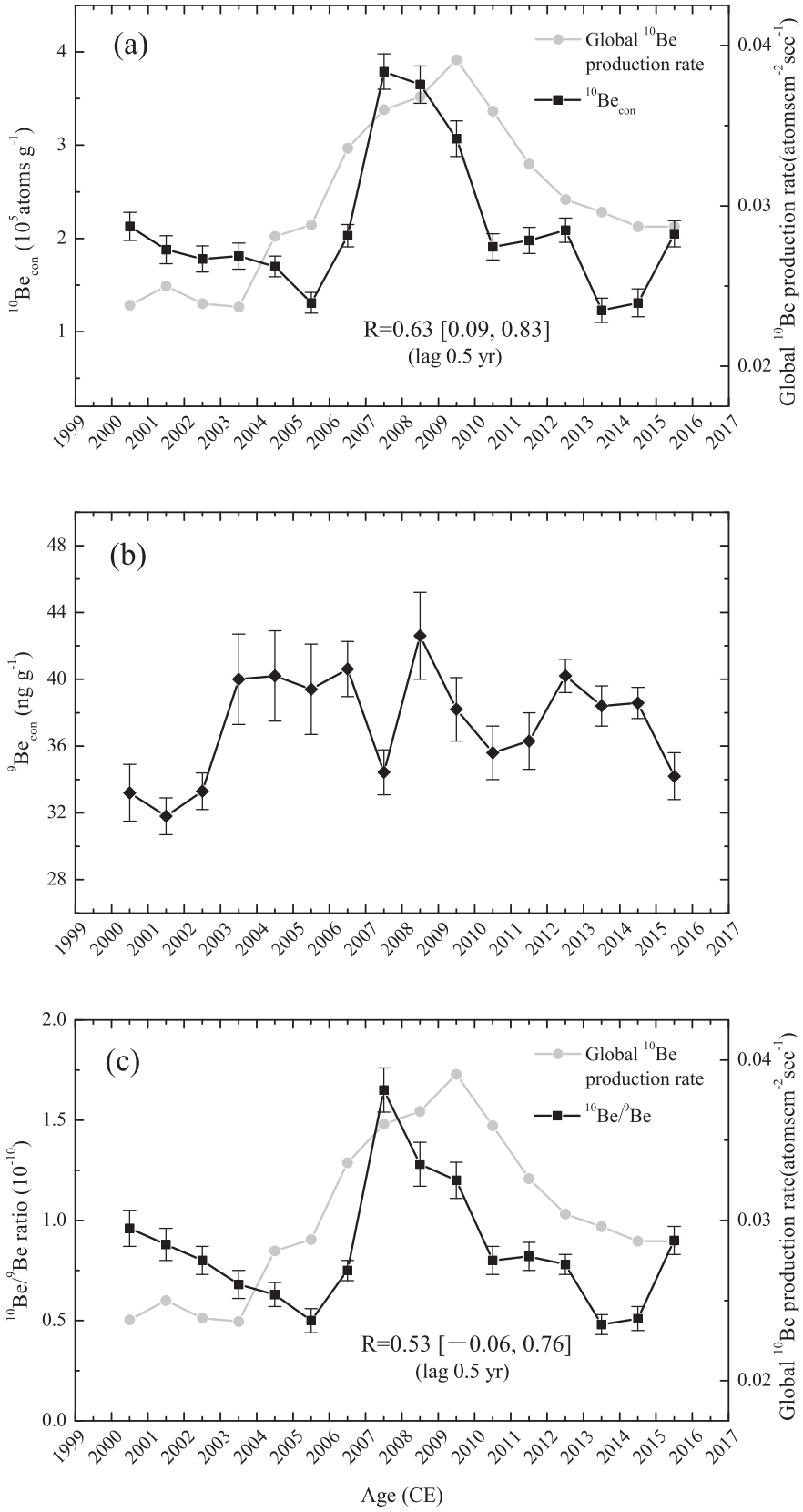

Fig. 4. (a) Travertine ^{10}Be concentration (^{10}Be$_{con}$) during the period 2001–2016 compared with the global ^{10}Be production rate calculated based on the ^{10}Be production model from Poluianov et al. (2016) and the annual solar modulation potential provided by Usoskin et al. (2011); (b) The variation of ^{9}Be concentration (^{9}Be$_{con}$) in the travertine sample for the same period; (c) Travertine ^{10}Be/^{9}Be ratio compared with the global ^{10}Be production rate. Note that the ^{10}Be, ^{9}Be and ^{10}Be/^{9}Be series are shifted by a half year into the past according to the lag analysis (See Supplement 3). Correlation coefficient is indicated together with the 95% confidence intervals CI).

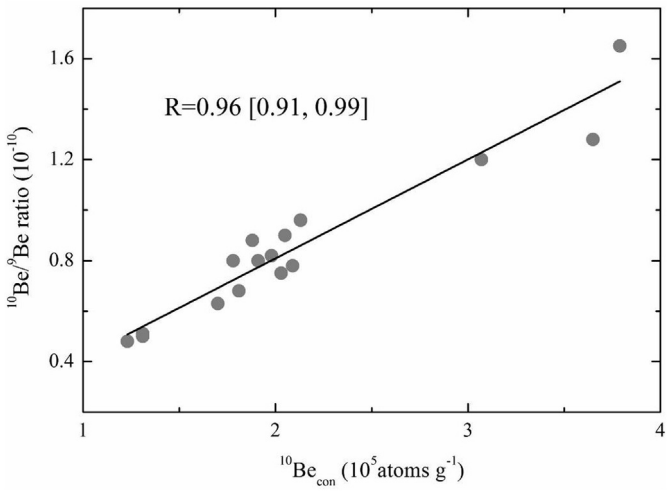

Fig. 5. The scatter diagrams of annual $^{10}Be_{con}$ and $^{10}Be/^{9}Be$ ratio in travertine during the period 2001–2016. The correlation coefficient is indicated together with the 95% confidence intervals.

from seasonally different travertine accumulation rates (Miyahara et al., 2018, under review). The annual precipitation around the sampling site has obvious seasonal variation, that is, more precipitation in summer and autumn, and less precipitation in winter and spring. Spring water, as a stable water source containing Ca^{2+} and HCO_3^-, has played a major role in Baishuitai travertine deposition. Higher precipitation in the rainy season therefore reduce the concentration of Ca^{2+} and HCO_3^- and result in lower accumulation rate of travertine. On the other hand, low local precipitation in dry season will enhance the concentration of Ca^{2+} and HCO_3^- and cause higher travertine accumulation rate (Liu et al., 2010). When the travertine accumulation rate is high, ^{10}Be in the travertine layer is diluted and its concentration becomes low. On the contrary, the low accumulation rate during the rainy season causes high ^{10}Be concentration in the travertine layer. Accordingly, ^{10}Be concentrations in the newly formed travertines vary with the season.

It has been reported that normalization of ^{10}Be content against the concentration of the stable isotope ^{9}Be is effective in minimizing the influence of variations in sediments accumulation rate (Carcaillet et al., 2004; Leduc et al., 2006; Ménabréaz et al., 2011; Horiuchi et al., 2016), and it has been reported that it is also applicable to the travertine deposits (Miyahara et al., 2018, under review). We therefore applied this methodology also in this study. Fig. 4b shows the variation of ^{9}Be concentration in travertine during the same period. Fig. 5 reveals a highly significant correlation between $^{10}Be/^{9}Be$ and $^{10}Be_{con}$ ($R = 0.96$ with 95% CI of 0.91–0.99) for all the dry season (white) layers. Given that the dry season has approximately only 10 percent of the precipitation that falls in the rainy season, the impact of changes in accumulation rate of the white layers on the ^{10}Be concentration appears to be relatively weak. Though that impact is relatively weak, it is still necessary to make a correction by using ^{9}Be since we are not sure of the exact months contained in each of these white layers according to the sub-sampling method as described in Fig. 2c and Supplement 1.

However, the correlation coefficient between $^{10}Be/^{9}Be$ and the global ^{10}Be production rate ($R = 0.53$ with 95% CI of - 0.06 to 0.76 with a time lag of 0.5 yr) (Fig. 4c) is somewhat lower than that between $^{10}Be_{con}$ and the global ^{10}Be production rate, suggesting that at least some other depositional effects need to be taken into consideration.

3.3. The effect of overland flow and its correction

3.3.1. The effect of overland flow on ^{10}Be concentrations

In addition to the accumulation rate effect, overland flow can be an important factor on ^{10}Be concentration in travertine. When upwelling S3 spring water enters the artificial canal, and forms travertine through CO_2 degassing, quantities of mineral soils and organics derived from the catchment are incorporated as an

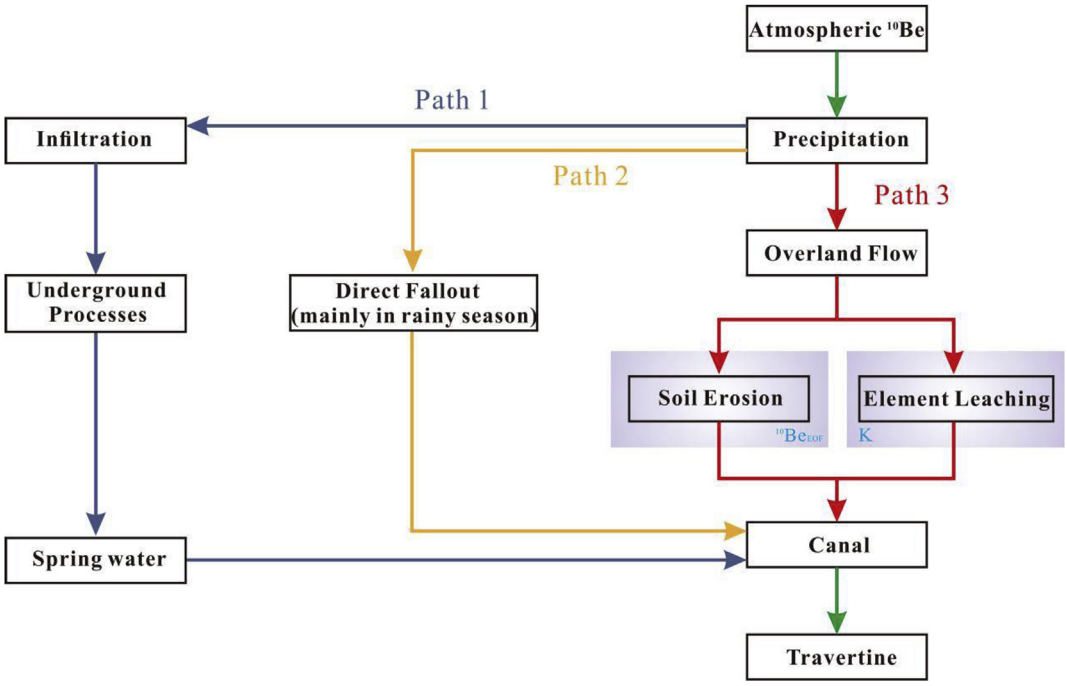

Fig. 6. A schematic diagram of the depositional processes of ^{10}Be into travertine. There are three possible paths for the ^{10}Be transportation into the canal; transportation by the groundwater (Path 1), direct fallout by the precipitation (Path 2), and by the overland flow that deliver eroded soils and sediments (Path 3).

overland flow (Liu et al., 2016). Due to its particle affinity, ^{10}Be tends to be absorbed onto the surface of soil constituents (Gu et al., 1996, 1997; Willenbring and von Blanckenburg, 2010). Therefore, ^{10}Be attached to such particles enters the canal during overland flow and impacts on ^{10}Be values in the travertine.

In order to account for such additional sources, the depositional processes of ^{10}Be during the dry season must be considered. There are three possible sources of ^{10}Be during dry season conditions: the spring water, local rainfall, and soils and sediments transported by the overland flow (Fig. 6). The S3 spring is supplied by regional precipitation that penetrates the ground; it is perennial and stable (Sun and Liu, 2010) and, since it is regarded as the main contributor to ^{10}Be in the travertine, we may assume that its ^{10}Be component reflects the atmospheric radionuclide production signal. Because rainfall during the dry season is very low as mentioned in 3.2, it contributes only negligible amounts of ^{10}Be. On the other hand, the contribution of ^{10}Be from sediments transported by the overland flow (Path 3 in Fig. 6) varies greatly with local climate and environmental conditions and, as such, needs to be more carefully studied in terms of its possible impact on the travertine ^{10}Be record.

3.3.2. Potassium correction

We hypothesize that sediment transportation by the overland flow may be monitored by the content of soluble elements such as K and Fe in the travertine. By the correlation analysis between the soluble elements and the precipitation rate, we found that the potassium (K) content show a significant correlation to the dry season precipitation (For the detailed information, See Supplement

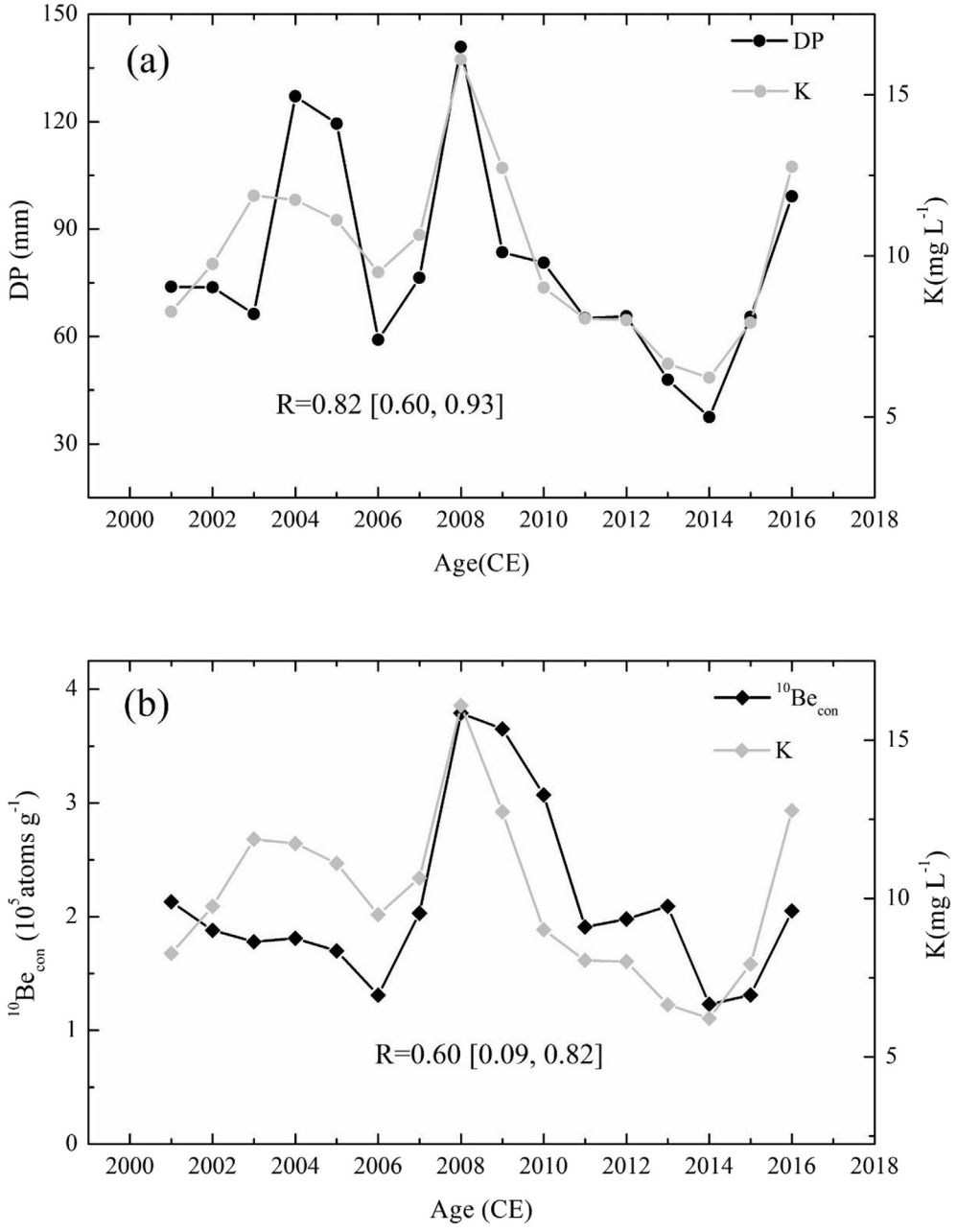

Fig. 7. (a) Potassium (K) content in travertine compared to local dry season precipitation (DP) during the period 2001–2016; (b) Potassium (K) content in travertine compared to ^{10}Be concentration (^{10}Be$_{con}$) in the same archive during the period 2001–2016. The correlation coefficient (R) between two parameters is indicated together with the 95% confidence interval.

4). Fig. 7a indicates the correlation between K content in the travertine and the local dry season precipitation (DP) (R = 0.82 with 95% CI of 0.60–0.93). The K content in S3 spring water is extremely limited (Liu et al., 2016), and its source in travertine is therefore predominantly from overland flow. Fig. 6 exhibits a possible explanation for the relationship between K and local precipitation. Heavy local precipitation events during the dry season result in overland flow, which, delivers entrained soil materials through erosion in the catchment area, and at the same time, leaches soluble elements through destruction of soil mineral lattice. Following its overland flow, both soil materials and soluble elements enter in the canal and are incorporated into the travertine. Where such materials in the catchment are homogeneous, the elemental content is directly proportional to the strength of overland flow, which in turn is related to the amount of local precipitation. Thus, the significant correlation between K and local precipitation (Fig. 7a) suggests that variations in K content reflect the overland flow discharge resulting from local precipitation, and that the ^{10}Be contamination caused by soil erosion may be corrected using the K content.

In fact, there is a significant correlation between K and $^{10}Be_{con}$ (R = 0.60 with 95% CI of 0.09–0.82) in the Baishuitai travertine and both series show a similar peak in 2008 (Fig. 7b). According to meteorological data from the meteorological station of Shangri-La (Fig. 1), dry season precipitation (from Nov. 2007 to Apr. 2008) was the highest of the recent 15 dry seasons. These results suggest that there is indeed a^{10}Be component brought by the effect of overland flow ($^{10}Be_{EOF}$) and that this would also accumulate in the travertine. $^{10}Be_{EOF}$ tends to be absorbed into soil surface, and soil material and soluble elements are delivered into canal as an overland flow, which mean both $^{10}Be_{EOF}$ and K experience the same transport processes of the ground surface prior to their accumulation in the travertine. Considering the significant correlation between K and $^{10}Be_{con}$, regression analysis of the ^{10}Be/^{9}Be time-series with K in travertine can be used to account for, and estimate, the ^{10}Be component due to the effect of overland flow ($[^{10}Be/^{9}Be]_{EOF}$). Linear regression of the ^{10}Be/^{9}Be time-series with K content is shown in Fig. 8 (for the full list of data sets, see Supplement 5). The resulting equations are as follows:

$$[^{10}Be/^{9}Be]_{EOF} = 0.1206 + 0.8794 \times K(norm) \quad (1)$$

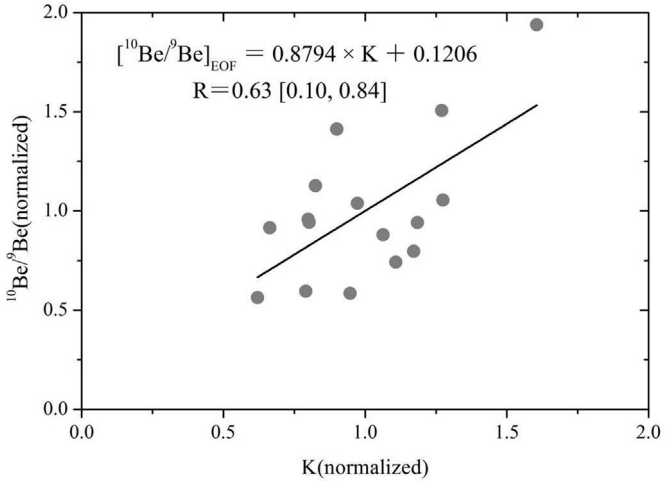

Fig. 8. Linear regression of annual ^{10}Be/^{9}Be ratio with potassium (K) content in travertine during the period 2001–2016. The correlation coefficient (R) between two parameters is indicated together with the 95% confidence interval.

An atmospheric ^{10}Be signal ($[^{10}Be/^{9}Be]_{ATM}$) can then be extracted by subtracting $[^{10}Be/^{9}Be]_{EOF}$ from ^{10}Be/^{9}Be ratio, and by adding the mean ^{10}Be/^{9}Be (norm) (value = 1) to calculate the relative amplitude variations:

$$\left[^{10}Be/^{9}Be\right]_{ATM} = {}^{10}Be/^{9}Be\ (norm) - {}^{10}Be/^{9}Be_{EOF} + 1 \quad (2)$$

Fig. 9a shows the results comparing corrected ^{10}Be content ($[^{10}Be/^{9}Be]_{ATM}$) with the global ^{10}Be production rate and reveals a good correlation. As a few years of time lag is expected due to the atmospheric transportation and the depositional processes, a lag analysis was performed on the $[^{10}Be/^{9}Be]_{ATM}$ time-series (Fig. 9b). We find that the most significant correlation between the $[^{10}Be/^{9}Be]_{ATM}$ and the global ^{10}Be production rate is observed at a time lag of 1.5–2.5 yrs (lag 1.5 yrs: R = 0.71 with 95% CI of 0.41–0.91; lag 2.5 yrs: R = 0.71 with 95% CI of 0.34–0.92) (Fig. 9b). The residence time of ^{10}Be in atmosphere is well established and known to be 1–2 years (Raisbeck et al., 1981a). On the other hand, the time scale of the underground process in Baishuitai is not well established; however, recent research suggests that it shows short groundwater residence times (less than 1yr) in the other typical of karst terrains, southwest China (Zhao et al., 2018). It supports that the groundwater circulation process in the southwest region of China is relatively rapid. The overall time lag of 1.5–2.5 yrs observed between the $[^{10}Be/^{9}Be]_{ATM}$ in travertine and the global ^{10}Be production rate is therefore consistent with the expected delay in the atmospheric transportation and the depositional process.

Our results suggest that the amplitude of ^{10}Be variation obtained from the travertine is approximately ±43% (Fig. 9c). The theoretically estimated amplitudes of the global atmospheric ^{10}Be production rate are about ±25% (Usoskin et al., 2011) or ±22% (Gieseler et al., 2017) over the same period. The amplitude of travertine ^{10}Be variation is nearly 1.7 times as much as the maximum theoretically estimated amplitude. This cannot be explained unless a predominant input of polar air-mass to the sampling site (~30°N) would occur. We therefore expect that there is a possibility that there are yet an unremoved local climatic or environmental impacts overlaid to the atmospheric production signal obtained in this study. Previous annual ^{10}Be record from lake sediment or ice core have also shown a relatively larger amplitude variation compared to the theoretical estimates (Pedro et al., 2011; Czymzik et al., 2015). Pedro et al. (2012) have shown that stacking multiple records would efficiently enhance the signal to noise ratio and enable a reconstruction with comparable amplitude to the theoretically estimated signal. Our correction method using K also effectively reduce the variability of ^{10}Be time series; however, we assume that our method to correct the climatic impact may need further improvement.

In conclusion, our data analysis supports that the Baishuitai travertine ^{10}Be record reflects changes in atmospheric radionuclide production as modulated by solar activity. For the establishment of travertine ^{10}Be as a new high-resolution proxy for the past cosmic ray and solar activity variations, further researches of travertines especially around Baishuitai area are encouraged.

4. Concluding remarks

We constructed an annual ^{10}Be record from endogenic travertine in Baishuitai, China, covering the period 2001–2016 CE, and explored its potential as a proxy of the past solar activity. The following conclusions were obtained in this study:

1. The annual $^{10}Be_{con}$ varies between 1.23 ± 0.13 and $3.79 \pm 0.19 \times 10^5$ atoms g^{-1}, with a mean of $2.11 \pm 0.15 \times 10^5$ atoms g^{-1}. The approximate $^{10}Be_{flux}$ values are consistent with

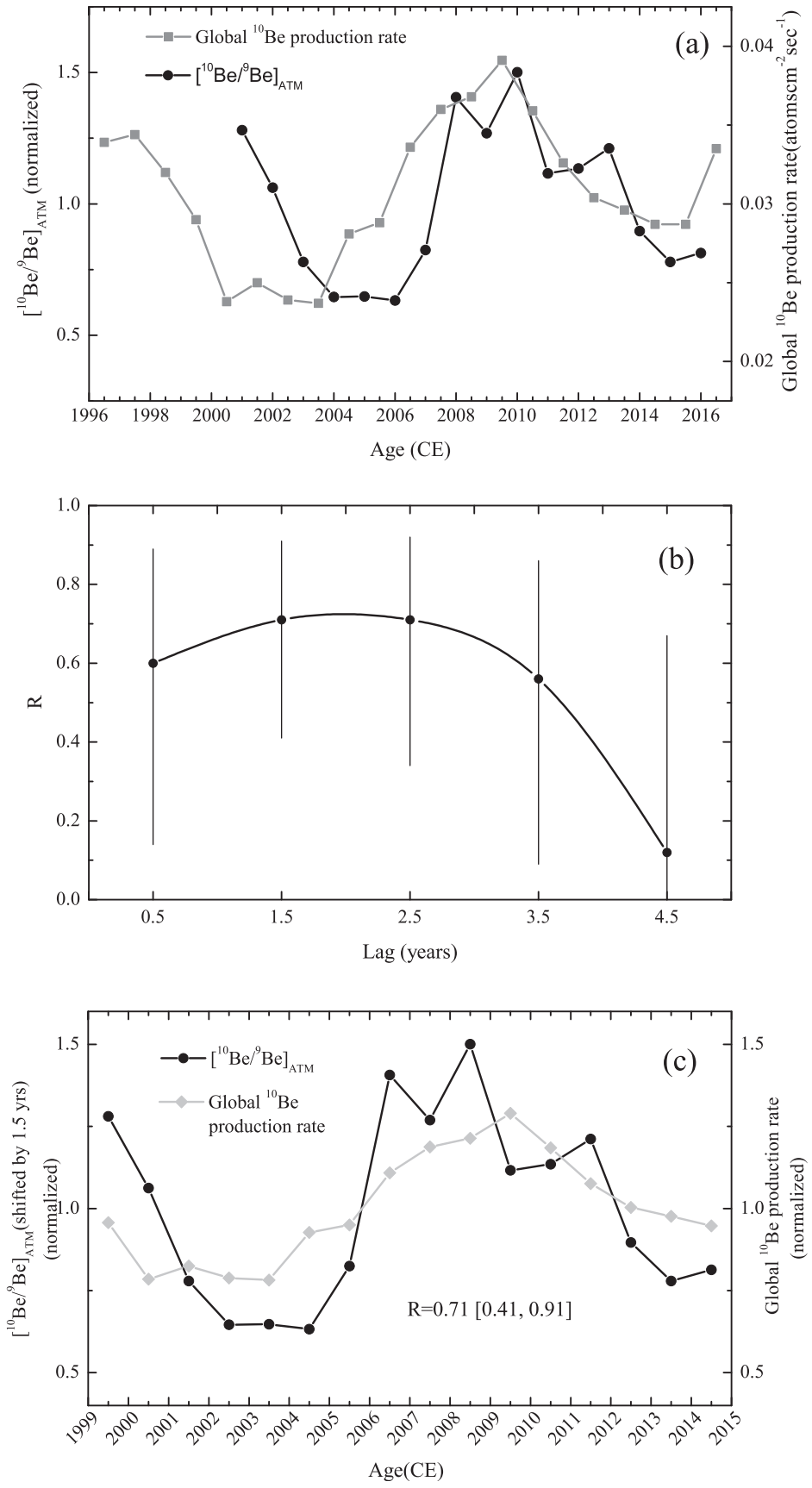

Fig. 9. (a) Corrected travertine ^{10}Be content ($[^{10}Be/^{9}Be]_{ATM}$) compared with the global ^{10}Be production rate calculated based on the solar modulation parameter by Usoskin et al. (2011). Note that the central age of dry-season travertine layers and the annual global ^{10}Be production rate differs by 0.5 years. (b) Time-lag analysis between $[^{10}Be/^{9}Be]_{ATM}$ and the global ^{10}Be production rate. Error bars show the 95% confidence intervals. (c) The variation of $[^{10}Be/^{9}Be]_{ATM}$ shifted by 1.5 yrs into the past, compared to the global ^{10}Be production rate.

the theoretically estimated deposition flux of atmospheric ^{10}Be around the sampling site.

2. The $^{10}Be_{con}$ correlates with the global ^{10}Be production rate ($R = 0.63$ with 95% CI of 0.09–0.83), reflecting the atmospheric radionuclide production signal.
3. Changing accumulation rate of carbonate and the impacts from the overland flow are the main factors that should be corrected to obtain accurate atmospheric ^{10}Be production signal. We conclude that it is feasible by using ^{9}Be and K to correct the effects of the accumulation rate and the overland flow, respectively.
4. The corrected ^{10}Be record shows higher correlation coefficient with the global ^{10}Be production rate than the original ^{10}Be record with a time lag of 1.5–2.5 years. The amplitude of travertine ^{10}Be variation is, however, nearly 1.7 times as much as the maximum theoretically estimated amplitude, which may be resulted from the local climatic or environmental impacts that could not be corrected by the method explored in this study.

In summary, the high correlation coefficient between the global ^{10}Be production rate and the ^{10}Be obtained from the Baishuitai travertine suggests a high potential of this carbonate sediment as an archive of the past solar activity and cosmic-ray variations, although there remain some uncertainties in our understandings of depositional process of ^{10}Be into travertine as well as the climatic and environmental impacts. The climate and surrounding environment of Baishuitai entails that its travertine deposits have clearly visible annual layers, and suggest that travertine may facilitate the reconstruction of past solar activity and cosmic-ray variations with definitive annual resolution. Further investigations are needed to the further refinement of ^{10}Be record obtained from the travertine at Baishuitai.

Acknowledgements

We would like to thank the two anonymous reviewers for their helpful comments and suggestions. This work was supported by NSFC grant number 41571040, 41761144062 and JSPS KAKENHI Grant Number 15K13488, 15H05816, 15K21709, 25287051, 25247082, 15K13581, and 19H00706. This work was also supported by the open research funding by LASG and CAS. We thank Dr. Hao Yan, Mr. Jirong He for their help in sampling, and we also thank Prof. Michael Meadows for his careful reading of the manuscript.

Appendix A. Supplementary data

Supplementary data to this article can be found online at https://doi.org/10.1016/j.quascirev.2019.05.012.

References

Andrews, J.E., 2006. Palaeoclimatic records from stable isotopes in riverine tufas: synthesis and review. Earth-Sci. Rev. 75, 85–104. http://doi.org/10.1016/j.earscirev.2005.08.002.

Bard, E., Raisbeck, G.M., Yiou, F., Jouzel, J., 1997. Solar modulation of cosmogenic nuclide production over the last millennium: comparison between 14C and 10Be records. Earth Planet. Sc. Lett. 150, 453–462. https://doi.org/10.1016/S0012-821X(97)00082-4.

Baroni, M., Bard, E., Petit, J., Magand, O., Bourlès, D., 2011. Volcanic and solar activity, and atmospheric circulation influences on cosmogenic 10Be fallout at Vostok and Concordia (Antarctica) over the last 60 years. Geochim. Cosmochim. Ac. 75, 7132–7145. https://doi.org/10.1016/j.gca.2011.09.002.

Beer, J., Siegenthaler, U., Bonani, G., Finkel, R.C., Oeschger, H., Suter, M., Wolfli, W., 1988. Information on past solar activity and geomagnetism from 10Be in the Camp Century ice core. Nature 331, 675–679. https://doi.org/10.1038/331675a0.di.

Beer, J., Blinov, A., Bonani, G., Finkel, R.C., Hofmann, H.J., Lehmann, B., Oeschger, H., Sigg, A., Schwander, J., Staffelbach, T., Stauffer, B., Suter, M., Wötfli, W., 1990. Use of 10Be in polar ice to trace the 11-year cycle of solar activity. Nature 347, 164–166. http://doi.org/10.1038/347164a0.

Beer, J., 2000. Long-term indirect indices of solar variability. Space Sci. Rev. 94, 53–66. https://doi.org/10.1023/a:1026778013901.

Beer, J., Vonmoos, M., Muscheler, R., 2006. Solar variability over the past several millennia. Space Sci. Rev. 125, 67–79. http://doi.org/10.1007/s11214-006-9047-4.

Beer, J., McCracken, K.G., Abreu, J., Heikkilä, U., Steinhilber, F., 2013. Cosmogenic radionuclides as an extension of the neutron monitor era into the past: potential and limitations. Space Sci. Rev. 176, 89–100. http://doi.org/10.1007/s11214-011-9843-3.

Berggren, A.M., Beer, J., Possnert, G., Aldahan, A., Kubik, P., Christl, M., Johnsen, S.J., Abreu, J., Vinther, B.M., 2009. A 600-year annual 10Be record from the NGRIP ice core. Greenland. Geophys. Res. Lett. 36, L11801. http://doi.org/10.1029/2009GL038004.

Berggren, A.M., Aldahan, A., Possnert, G., Haltia-Hovi, E., Saarinen, T., 2010. 10Be and solar activity cycles in varved lake sediments, AD 1900–2006. J. Paleolimnol. 44, 559–569. http://doi.org/10.1007/s10933-010-9437-1.

Berggren, A.M., Aldahan, A., Possnert, G., Haltia-Hovi, E., Saarinen, T., 2013. Linking ice sheet and lake sediment archives of 10Be, 1468–1980 CE. Nucl. Instrum. Meth. B. 294, 524–529. http://doi.org/10.1016/j.nimb.2012.05.024.

Carcaillet, J.T., Bourle, D.L., Thouveny, N., Arnold, M., 2004. A high resolution authigenic 10Be/9Be record of geomagnetic moment variations over the last 300 ka from sedimentary cores of the Portuguese margin. Earth Planet. Sc. Lett. 219, 397–412. http://doi.org/10.1016/S0012-821X(03)00702-7.

Cauquoin, A., Raisbeck, G.M., Jouzel, J., Bard, E., 2014. No evidence for planetary influence on solar activity 330 000 years ago. Astron. Astrophys. 561, A132. http://doi.org/10.1051/0004-6361/201322879.

Czymzik, M., Muscheler, R., Brauer, A., Adolphi, F., Ott, F., Kienel, U., Dräger, N., Słowiński, M., Aldahan, A., Possnert, G., 2015. Solar cycles and depositional processes in annual 10Be from two varved lake sediment records. Earth Planet. Sc. Lett. 428, 44–51. http://doi.org/10.1016/j.epsl.2015.07.037.

Czymzik, M., Adolphi, F., Muscheler, R., Mekhaldi, F., Martin-Puertas, C., Aldahan, A., Possnert, G., Brauer, A., 2016. A varved lake sediment record of the 10Be solar activity proxy for the Lateglacial-Holocene transition. Quaternary Sci. Rev. 153, 31–39. http://doi.org/10.1016/j.quascirev.2016.10.007.

Czymzik, M., Muscheler, R., Adolphi, F., Mekhaldi, F., Dräger, N., Ott, F., Słowinski, M., Błaszkiewicz, M., Aldahan, A., Possnert, G., Brauer, A., 2018. Synchronizing 10Be in two varved lake sediment records to IntCal13 14C during three grand solar minima. Clim. Past. 14, 687–696. http://doi.org/10.5194/cp-14-687-2018.

Dansgaard, W., 1964. Stable isotopes in precipitation. Tellus 16, 436–468. https://doi.org/10.3402/tellusa.v16i4.8993.

Delaygue, G., Bard, E., 2010. An Antarctic view of Beryllium-10 and solar activity for the past millennium. Clim. Dynam. 36, 2201–2218. http://doi.org/10.1007/s00382-010-0795-1.

Ford, T.D., Pedley, H.M., 1996. A review of tufa and travertine deposits of the world. Earth-Sci. Rev. 41, 117–175. https://doi.org/10.1016/S0012-8252(96)00030-X.

Gieseler, J., Heber, B., Herbst, K., 2017. An empirical modification of the force field approach to describe the modulation of galactic cosmic rays Close to earth in a broad range of rigidities. J. Geophys. Res-Space. 122 (10), 910–964, 979. http://doi.org/10.1002/2017JA024763.

Gray, L.J., Beer, J., Geller, M., Haigh, D.J., M, L, Matthes, K., Cubasch, U., Fleitmann, D., Harrison, G., Hood, L., Luterbacher, J., Meehl, A.G., Shindell, D., Van Geel, B., A.W.W., 2010. Solar influences on climate. Rev. Geophys. 48, G4001. https://doi.org/10.1029/2009RG000282.

Gu, Z.Y., La, D., Liu, T.S., Southon, J., Caffee, M.W., Guo, Z.T., Y, C.M., 1996. Five million year loBe record in Chinese loess and red-clay: climate and weathering relationships. Earth Planet. Sc. Lett. 144, 273–287. https://doi.org/10.1016/0012-821X(96)00156-2.

Gu, Z.Y., Lal, D., Liu, T.S., Guo, Z.T., Southon, J., Caffee, M.W., 1997. Weathering histories of Chinese loess deposits based on uranium and thorium series nuclides and cosmogenic 10Be. Geochim. Cosmochim. Ac. 61, 5221–5231. https://doi.org/10.1016/S0016-7037(97)00313-X.

Heikkila, U., Beer, J., Abreu, J.A., Steinhilber, F., 2011. On the atmospheric transport and deposition of the cosmogenic radionuclides (10Be): a review. Space Sci. Rev. 176, 321–332. http://doi.org/10.1007/s11214-011-9838-0.

Horiuchi, K., Goldberg, E.L., Kobayashi, K., Oda, T., Nakamura, T., Kawai, T., 2001. Climate-induced variations of cosmogenic beryllium-10 in the sediments of Lake Baikal of the last 150 ky from AMS, SRXRF and NAA data. Nucl. Instrum. Meth. A. 470, 396–404. https://doi.org/10.1016/S0168-9002(01)01085-3.

Horiuchi, K., Matsuzaki, H., Kobayashi, K., Goldberg, E.L., 2003. 10Be record and magnetostratigraphy of a Miocene section from Lake Baikal: Re-examination of the age model and its implication for climatic changes in continental Asia. Geophys. Res. Lett. 30. https://doi.org/10.1029/2003GL017488.

Horiuchi, K., Uchida, T., Sakamoto, Y., Ohta, A., Matsuzaki, H., Shibata, Y., Motoyama, H., 2008. Ice core record of 10Be over the past millennium from Dome Fuji, Antarctica: a new proxy record of past solar activity and a powerful tool for stratigraphic dating. Quat. Geochronol. 3, 253–261. http://doi.org/10.1016/j.quageo.2008.01.003.

Horiuchi, K., Oniyanagi, I., Wasada, H., Matsuzaki, H., 2013. 10Be measurements at MALT using reduced-size samples of bulk sediments. Nucl. Instrum. Meth. B. 294, 72–76. https://doi.org/10.1016/j.nimb.2012.06.022.

Horiuchi, K., Matsuzaki, H., 2015. Exploration of 10Be analysis using 10 μg of Be carrier. Nucl. Instrum. Meth. B. 361, 423–430. https://doi.org/10.1016/j.nimb.2015.07.123.

Horiuchi, K., Kamata, K., Maejima, S., Sasaki, S., Sasaki, N., Yamazaki, T., Fujita, S.,

Motoyama, H., Matsuzaki, H., 2016. Multiple 10Be records revealing the history of cosmic-ray variations across the Iceland Basin excursion. Earth Planet. Sc. Lett. 440, 105–114. http://doi.org/10.1016/j.epsl.2016.01.034.
Inceoglu, F., Knudsen, M.F., Olsen, J., Karoff, C., Herren, P.A., Schwikowski, M., Aldahan, A., Possnert, G., 2016. A continuous ice-core 10Be record from Mongolian mid-latitudes: influences of solar variability and local climate. Earth Planet. Sc. Lett. 437, 47–56. http://doi.org/10.1016/j.epsl.2016.01.006.
Lal, D., Peters, B., 1967. Cosmic Ray Produced Radioactivity on the Earth. Springer Berlin Heidelberg. https://doi.org/10.1007/978-3-642-46079-1_7.
Leduc, G., Thouveny, N., Bourles, D., Blanchet, C., Carcaillet, J., 2006. Authigenic 10Be/9Be signature of the Laschamp excursion: a tool for global synchronisation of paleoclimatic archives. Earth Planet. Sc. Lett. 245, 19–28. http://doi.org/10.1016/j.epsl.2006.03.006.
Liu, Z., Zhang, M., Li, Q., You, S., 2003. Hydrochemical and isotope characteristics of spring water and travertine in the Baishuitai area (SW China) and their meaning for paleoenvironmental reconstruction. Environ. Geol. 44, 698–704. http://doi.org/10.1007/s00254-003-0811-4.
Liu, Z.H., Li, Q., Sun, H.L., Liao, C.J., Li, H.J., Wang, J.L., Wu, K.Y., 2006. Diurnal variations of hydrochemistry in a travertine-depositing stream at Baishuitai, Yunnan, SW China. Aquat. Geochem. 12, 103–121. http://doi.org/10.1007/s10498-005-2962-2.
Liu, Z.H., Sun, H.L., Lu, B.Y., Liu, X.L., Ye, W.B., Zeng, C., 2010. Wet-dry seasonal variations of hydrochemistry and carbonate precipitation rates in a travertine-depositing canal at Baishuitai, Yunnan, SW China: implications for the formation of biannual laminae in travertine and for climatic reconstruction. Chem. Geol. 273, 258–266. http://doi.org/10.1016/j.chemgeo.2010.02.027.
Liu, Z.H., 2014. Research progress in paleoclimatic interpretations of tufa and travertine (in Chinese). Chin Sci Bull (Chin Ver). 59, 2229–2239. https://doi.org/10.1360/N972013-00037.
Liu, Z.H., Sun, H.L., Yan, H., Zhang, J.L., Wang, H.J., Zeng, H.T., 2016. Tufa/Travertine Investigations (in Chinese). Science Press, Beijing, ISBN 978-7-03-048745-2.
Ljung, K., Björck, S., Muscheler, R., Beer, J., Kubik, P.W., 2007. Variable 10Be fluxes in lacustrine sediments from Tristan da Cunha, South Atlantic: a solar record? Quaternary Sci. Rev. 26, 829–835. http://doi.org/10.1016/j.quascirev.2006.12.016.
Mann, M., Beer, J., Steinhilber, F., Christl, M., 2012. 10Be in lacustrine sediments—a record of solar activity? J. Atmos. Sol.-Terr. Phy. 80, 92–99. http://doi.org/10.1016/j.jastp.2012.03.011.
Matsuzaki, H., Nakano, C., Yamashita, H., Maejima, Y., Miyairi, Y., Wakasa, S., Horiuchi, K., 2004. Current status and future direction of MALT, the University of Tokyo. Nucl. Instrum. Meth. B. 223, 92–99. https://doi.org/10.1016/j.nimb.2004.04.022.
Matsuzaki, H., Nakano, C., Tsuchiya, Y.S., Ito, S., Morita, A., Kusuno, H., Miyake, Y., Honda, M., Bautista VII, A.T., Kawamoto, M., Tokuyama, H., 2015. The status of the AMS system at MALT in its 20th year. Nucl. Instrum. Meth. B. 361, 63–68. https://doi.org/10.1016/j.nimb.2015.05.032.
Ménabréaz, L., Thouveny, N., Bourlès, D.L., Deschamps, P., Hamelin, B., Demory, F., 2011. The Laschamp geomagnetic dipole low expressed as a cosmogenic 10Be atmospheric overproduction at ~41ka. Earth Planet. Sc. Lett. 312, 305–317. http://doi.org/10.1016/j.epsl.2011.10.037.
Mudelsee, M., 2003. Estimating pearson's correlation coefficient with bootstrap confidence interval from serially dependent time series. Math. Geol. 35, 651–665. https://doi.org/10.1023/B:MATG.0000002982.52104.02.
Muscheler, R., Adolphi, F., Herbst, K., Nilsson, A., 2016. The revised sunspot record in comparison to cosmogenic radionuclide-based solar activity reconstructions. Sol. Phys. 291, 3025–3043. http://doi.org/10.1007/s11207-016-0969-z.
Nishiizumi, K., Imamura, M., Caffee, M.W., Southon, J.R., Finkel, R.C., McAninch, J., 2007. Absolute calibration of 10Be AMS standards. Nucl. Instrum. Meth. B. 258, 403–413. https://doi.org/10.1016/j.nimb.2007.01.297.
Pedro, J.B., Smith, A.M., Simon, K.J., van Ommen, T.D., Curran, M.A.J., 2011. High-resolution records of the beryllium-10 solar activity proxy in ice from Law Dome, East Antarctica: measurement, reproducibility and principal trends. Clim. Past. 7, 707–721. http://doi.org/10.5194/cp-7-707-2011.
Pedro, J.B., McConnell, J.R., van Ommen, T.D., Fink, D., Curran, M.A.J., Smith, A.M., Simon, K.J., Moy, A.D., Das, S.B., 2012. Solar and climate influences on ice core 10Be records from Antarctica and Greenland during the neutron monitor era. Earth Planet. Sc. Lett. 355–356, 174–186. http://doi.org/10.1016/j.epsl.2012.08.038.
Pentecost, A., 1995. The quaternary travertine deposits of europe and Asia minor. Quaternary Sci. Rev. 14, 1005–1028. https://doi.org/10.1016/0277-3791(95)00101-8.
Poluianov, S.V., Kovaltsov, G.A., Mishev, A.L., Usoskin, I.G., 2016. Production of cosmogenic isotopes 7Be, 10Be, 14C, 22Na, and 36Cl in the atmosphere: altitudinal profiles of yield functions. J. Geophys. Res-Atmos. 121, 8125–8136. http://doi.org/10.1002/2016JD025034.
Raisbeck, G.M., Yiou, F., Fruneau, M., Loiseaux, J.M., Lieuvin, M., Ravel, J.C., 1981a. Cosmogenic Be-10/Be-7 as a probe of atmospheric transport processes. Geophys. Res. Lett. 8, 1015–1018. https://doi.org/10.1029/GL008i009p01015.
Raisbeck, G.M., Yiou, F., Fruneau, M., Loiseaux, J.M., Lieuvin, M., Ravel, J.C., Lorius, C., 1981b. Cosmogenic 10Be concentrations in Antarctic ice during the past 30,000 years. Nature 292, 825–826. https://doi.org/10.1038/292825a0.
Steinhilber, F., Abreu, J., Beer, J., Brunner, I., Christl, M., Fischer, H., Heikkilä, U., Kubik, P., Mann, M., McCracken, K.G., Miller, H., Miyahara, H., Oerterf, H., Wilhelms, F., 2012. 9,400 years of cosmic radiation and solar activity from ice cores and tree rings. Proc. Natl. Acad. Sci. 109, 5967–5971. http://doi.org/10.1073/pnas.1118965109.
Sun, H.L., Liu, Z.H., 2010. Wet–dry seasonal and spatial variations in the d13C and d18O values of the modern endogenic travertine at Baishuitai, Yunnan, SW China and their paleoclimatic and paleoenvironmental implications. Geochim. Cosmochim. Ac. 74, 1016–1029. http://doi.org/10.1016/j.gca.2009.11.008.
Sun, H.L., Liu, Z.H., Yan, H., 2014. Oxygen isotope fractionation in travertine-depositing pools at Baishuitai, Yunnan, SW China: effects of deposition rates. Geochim. Cosmochim. Ac. 133, 340–350. http://doi.org/10.1016/j.gca.2014.03.006.
Usoskin, I.G., Bazilevskaya, G.A., Kovaltsov, G.A., 2011. Solar modulation parameter for cosmic rays since 1936 reconstructed from ground-based neutron monitors and ionization chambers. J. Geophys. Res. 116, A2104. http://doi.org/10.1029/2010JA016105.
Usoskin, I.G., 2017. A history of solar activity over millennia. Living Rev. Sol. Phys. 14, 1–97. http://doi.org/10.1007/s41116-017-0006-9.
Vonmoos, M., Beer, J., Muscheler, R., 2006. Large variations in Holocene solar activity: constraints from 10Be in the Greenland ice core project ice core. J. Geophys. Res. 111, A10105. http://doi.org/10.1029/2005JA011500.
Willenbring, J.K., von Blanckenburg, F., 2010. Meteoric cosmogenic Beryllium-10 adsorbed to river sediment and soil: applications for Earth-surface dynamics. Earth-Sci. Rev. 98, 105–122. http://doi.org/10.1016/j.earscirev.2009.10.008.
Wu, C.J., Usoskin, I.G., Krivova, N., Kovaltsov, G.A., Baroni, M., Bard, E., Solanki, S.K., 2018. Solar activity over nine millennia: a consistent multi-proxy reconstruction. Astron. Astrophys. 615, A93. http://doi.org/10.1051/0004-6361/201731892.
Yamaguchi, Y., Yokoyama, Y., Miyahara, H., Sho, K., Nakatsuka, T., 2010. Synchronized Northern Hemisphere climate change and solar magnetic cycles during the Maunder Minimum. Proc. Natl. Acad. Sci. 107, 20697–20702. http://doi.org/10.1073/pnas.1000113107.
Zhao, M., Hu, Y.D., Zeng, C., Liu, Z.H., Yang, R., Chen, B., 2018. Effects of land cover on variations in stable hydrogen and oxygen isotopes in karst groundwater: a comparative study of three karst catchments in Guizhou Province, Southwest China. J. Hydrol. 565, 374–385. http://doi.org/10.1016/j.jhydrol.2018.08.037.
Zhao, X.T., Li, T., He, S., 1998. The Baishuitai of China (in Chinese). Tourism Press of China, Beijing, ISBN 7-5032-1507-0.